

Impact of end-capped groups on the properties of dithienosilole-based small molecules for solution-processed organic solar cells

Xianjie Chen ^a, Huanran Feng ^b, Zhijing Lin ^a, Zhaowei Jiang ^a, Tian He ^a, Shouchun Yin ^a, Xiangjian Wan ^b, Yongsheng Chen ^b, Qian Zhang ^{a,*}, Huayu Qiu ^{a,**}

^a College of Material, Chemistry and Chemical Engineering, Hangzhou Normal University, Hangzhou 310036, China

^b The Centre of Nanoscale Science and Technology and Key Laboratory of Functional Polymer Materials, State Key Laboratory and Institute of Elemento Organic Chemistry, Collaborative Innovation Center of Chemical Science and Engineering (Tianjin), College of Chemistry, Nankai University, Tianjin 300071, China

ARTICLE INFO

Article history:

Received 20 June 2017

Received in revised form

24 July 2017

Accepted 25 July 2017

Available online 27 July 2017

Keywords:

Small molecules

Organic solar cell

Dithienosilole

End-capped group

Morphology

ABSTRACT

Two new acceptor-donor-acceptor small molecules DINDTS and DINCNDTS, with dithienosilole as a core unit and 1,3-indanedione (IN) or malononitrile derivative 1,3-indanedione (INCN) units as end-capped groups, respectively, have been designed and synthesized for solution-processable bulk-heterojunction (BHJ) solar cells. The impact of these two end-capped groups on their optical, electrochemical properties and photovoltaic performance was systematically studied. The optimal DINDTS:PC₇₁BM based solar cells showed a short-circuit current density (J_{sc}) of 13.50 mA cm⁻² and power conversion efficiency (PCE) of 6.60%. However, DINCNDTS:PC₇₁BM based devices exhibited a poor PCE of 0.58% with a very low J_{sc} of 1.82 mA cm⁻², which are mainly due to its poor morphology of active layers.

© 2017 Elsevier Ltd. All rights reserved.

1. Introduction

Solution-processed bulk heterojunction (BHJ) organic solar cells (OSCs) have attracted intense attention due to their noteworthy merits, such as light weight, low cost, ease of large-area fabrication by roll-to-roll printing and flexibility [1]. Within recent years, the power conversion efficiencies (PCEs) have witnessed a rapid improvement with values surpassing 10% for both polymer and small-molecule based organic solar cells with fullerene derivatives as the acceptors [2–9]. The excellent performance of OSCs are attributed to novel photoactive material development and device optimization [10–13]. Compared to the conjugated polymers, small molecules possess some unique advantages, such as high purity, well-defined molecular structures, easier energy level control, simply synthetic procedures, and high reproducibility [14–16]. They are supposed to be good candidates for investigating the

chemical structure-photovoltaic performance relationships, which is highly important for further molecular design to achieve higher photovoltaic performance.

Among the reported various donor materials, polymers and small molecules containing (4,4'-bis(2-ethylhexyl)dithieno[3,2-*b*:2',3'-*d*]silole)-2,6-diyl (DTS) unit generally showed broad absorption, high hole mobility and good photovoltaic performance, which are derived from the highly planar molecular structure and good electron-donating ability of DTS unit. The DTS unit is a promising electron-donating building block for efficient donor materials for OSCs [17–20]. In addition, various processing techniques have been used to tune the morphology of the active layer in order to further improve the PCE of OSCs, such as the inclusion of solvent additives, thermal annealing and solvent annealing [21,22]. Among these techniques, it has been demonstrated that solvent vapor annealing (SVA) is an effective method to control the blend morphology and improve the short-circuit current density (J_{sc}), fill factor (FF) and PCE of OSCs [23–27]. Solvent vapor can penetrate into the blend inducing the re-organization of the donor and/or acceptor materials, and thus the crystallinity of the donors and the scale of the phase separation between donor and acceptor could be influenced.

* Corresponding author.

** Corresponding author.

E-mail addresses: qzhang@hznu.edu.cn (Q. Zhang), hyqiu@hznu.edu.cn (H. Qiu).

In this work, based on the above consideration, we have designed and synthesized two solution-processable small molecules DINDTS and DINCNDS, with DTS as the central electron-donating unit, 1,3-indanediene (IN) or 2-(3-oxo-2,3-dihydroinden-1-ylidene)malononitrile (INCN) as the terminal acceptor units, and thiophene as π -bridges (Fig. 1). The influence of different end-capped groups on the optical and electrochemical properties and device performance were systematically investigated. The two compounds possess good solubility in common organic solvents and high thermal stability. DINDTS and DINCNDS show broad absorption in the visible and near infrared region with absorption edges reaching 754 and 894 nm, respectively. The optimized devices based on DINDTS:PC₇₁BM exhibited a PCE of 6.60% with SVA treatment. However, the devices based on DINCNDS:PC₇₁BM achieved a low PCE of 0.58%, which mainly resulted from the poor morphology of active layers. Our study demonstrated that the end-capped acceptor units have great impact on the energy levels and active layer morphology, and thus the photovoltaic performance.

2. Materials and methods

2.1. Materials

All reactions and manipulations were carried out under an argon atmosphere using standard Schlenk techniques [6,6].-Phenyl-C₇₁-butyric acid methyl ester (PC₇₁BM) was purchased from American Dye Source, Inc. All starting materials were purchased from commercial suppliers and used without further purification unless indicated otherwise.

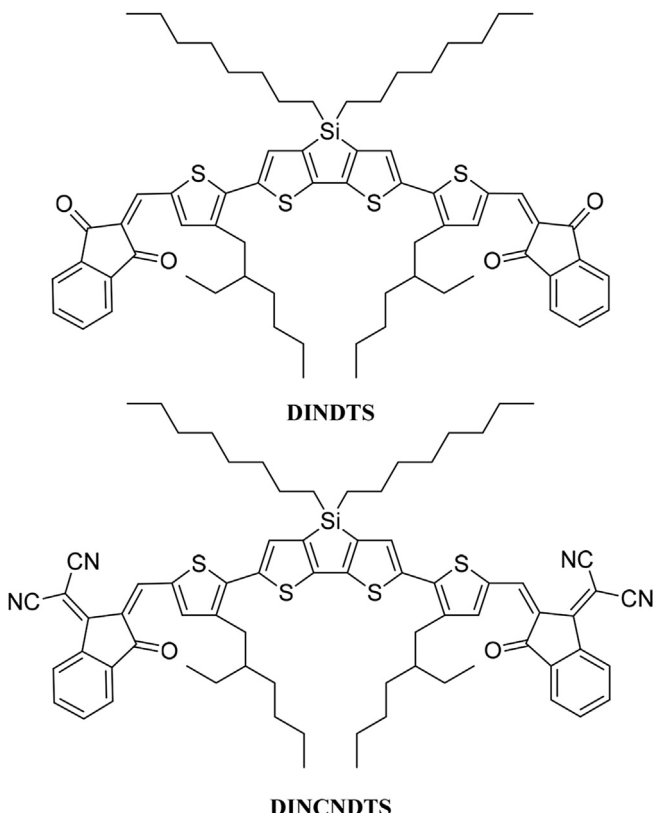


Fig. 1. Chemical structures of DINDTS and DINCNDS.

2.2. Instruments and measurements

¹H-NMR and ¹³C-NMR spectra were recorded on a Bruker AVANCE 500 spectrometer. HRMS was performed on Agilent 6530 Accurate-Mass Q-TOF LC/MS Spectrometer using Electro Spray Ionization (ESI) mode. Nicolet iS5 FT-IR Spectrometer was used to record IR spectra. The thermogravimetric analyses (TGA) and differential scanning calorimetric measurements (DSC) were carried out on a TA Q500 and a TA Q2000 instrument under nitrogen gas flow with a 10 °C min⁻¹ heating rate, respectively. UV-Vis absorption spectra were obtained with JASCO V-570 spectrophotometer. Cyclic voltammetry (CV) measurements were performed with a LK2005A electrochemical workstation in dry THF solution. All CV measurements were carried out at room temperature with a conventional three-electrode configuration employing a glassy carbon electrode as the working electrode, a saturated calomel electrode (SCE) as the reference electrode, and a Pt wire as the counter electrode. THF was distilled from calcium hydride under dry nitrogen immediately prior to use. Tetrabutylammonium phosphorus hexafluoride (Bu₄NPF₆, 0.1 M) in THF was used as the supporting electrolyte, and the scan rate was 100 mV s⁻¹.

Atomic force microscopy (AFM) was performed using Multi-mode 8 atomic force microscope in tapping mode. The transmission electron microscopy (TEM) investigation was performed on Philips Technical G² F20 at 200 kV. The specimen for TEM measurement was prepared by spin casting the blend solution on ITO/PEDOT:PSS substrate, then floating the film on a water surface, and transferred to TEM grids.

SCLC hole mobility was measured using a diode configuration of ITO/PEDOT:PSS/donor:PC₇₁BM/Au by taking the dark current density in the range of 0–8 V and fitting the results to a space charge limited form, where SCLC is described by:

$$J = \frac{9\epsilon_0\epsilon_r\mu_0 V^2}{8L^3} \exp\left(0.89\beta\sqrt{\frac{V}{L}}\right)$$

where J is the current density, L is the film thickness of the active layer, μ_0 is the hole or electron mobility, ϵ_r is the relative dielectric constant of the transport medium, ϵ_0 is the permittivity of free space (8.85×10^{-12} F m⁻¹), V (= $V_{\text{appl}} - V_{\text{bi}}$) is the internal voltage in the device, where V_{appl} is the applied voltage to the device and V_{bi} is the built-in voltage due to the relative work function difference of the two electrodes.

2.3. Fabrication and characterization of organic solar cells

The photovoltaic devices were fabricated with a structure of ITO/PEDOT:PSS/Donor:PC₇₁BM/ETL-1/Al. The ITO coated glass substrates were cleaned by ultrasonic treatment in detergent, deionized water, acetone, and isopropyl alcohol under ultrasonication for 15 min each and subsequently dried by a nitrogen blow. A thin layer of PEDOT:PSS (Clevios P VP Al 4083, filtered at 0.45 μ m) was spin-coated at 3000 rpm onto ITO surface. After baking at 150 °C for 20 min, the substrates were transferred into an argon-filled glove box. Subsequently, the active layer was spin-coated from blend chloroform solutions with weight ratio of donor and PC₇₁BM at 1:0.8 and then the substrates were placed in a glass petri dish containing 150 μ L chloroform for 70 s for solvent vapor annealing (SVA). Then the substrates were removed. And ETL-1 solution (0.5 mg/mL, dissolved in methanol) was spin-coated at 3000 rpm. Finally, 80 nm Al layer were deposited under high vacuum ($<2 \times 10^{-4}$ Pa). The effective areas of cells were 4 mm² defined by shallow masks. The current density-voltage (J - V) curves of photovoltaic devices were obtained by a Keithley 2400 source-

measure unit. All masked and unmasked tests gave consistent results with relative errors within 5%. The photocurrent was measured under illumination simulated 100 mW cm⁻² AM 1.5G irradiation using an Oriel 96000 solar simulator, calibrated with a standard Si solar cell. The average PCE was obtained using 50 devices under the same conditions. External quantum efficiencies were measured using Stanford Research Systems SR810 lock-in amplifier.

2.4. Synthesis

The synthetic routes of DINDTS and DINCNDS are shown in Scheme 1.

5,5'-(4,4-dioctyl-4H-silolo[3,2-*b*:4,5-*b'*]dithiophene-2,6-diyl)bis(4-(2-ethylhexyl)-thiophene-2-carbaldehyde) (DCHOTDTS): A solution of compound 1 (300.0 mg, 0.403 mmol) and compound 2 (488.9 mg, 1.612 mmol) in dry toluene (100 mL) was degassed twice with argon following the addition of $Pd(PPh_3)_4$ (186.0 mg, 0.161 mmol). After stirring and refluxing for 24 h at 110 °C with the protection of argon, the reaction mixture was poured into water (100 mL) and extracted with CH₂Cl₂ (100 mL × 2). The organic layer was washed with water for twice and dried over anhydrous MgSO₄ for 3 h. The solvent was removed by evaporation under reduced pressure. The crude product was purified by silica gel column chromatography with dichloromethane/petroleum ether (1:2) as eluent to afford compound DCHOTDTS (130.4 mg, 0.151 mmol, 37.5%) as oil. ¹H NMR (500 MHz, CD₂Cl₂) δ 9.74 (s, 2H), 7.50 (s, 2H), 7.23 (s, 2H), 2.70 (d, *J* = 7.3 Hz, 4H), 1.67–1.59 (m, 3H), 1.34–1.29 (m, 4H), 1.16 (d, *J* = 19.2 Hz, 35 H), 0.93–0.86 (m, 6 H), 0.77 (dd, *J* = 13.4, 7.1 Hz, 18H). ¹³C NMR (126 MHz, CD₂Cl₂) δ 182.46, 150.12, 143.74, 141.47, 140.07, 139.88, 139.61, 136.18, 130.62, 39.99, 33.63, 33.10, 32.48, 31.85, 29.68, 29.17, 29.14, 28.67, 25.69, 24.10, 23.03, 22.64, 13.87, 13.84, 11.64, 10.44. HRMS (ESI-TOF) *m/z*: calcd for C₅₀H₇₄O₂S₄Si[M]⁺, 863.4414; found, 863.4467.

2,2'-((4,4-dioctyl-4H-silolo[3,2-*b*:4,5-*b'*]dithiophene-2,6-diyl)bis(4-(2-ethylhexyl)-thiophene-5,2-diyl))bis(methanlylidene) bis(1*H*-indene-1,3(2*H*)-dione) (DINDTS): DCHOTDTS (100 mg, 0.116 mmol) and indandione (67.8 mg, 0.464 mmol) was dissolved in a dry CHCl₃ (30 mL) solution under the protection of argon, and then three drops of piperidine was added to the mixture. After stirring and refluxing for 12 h, the mixture was extracted with dichloromethane (50 mL × 2), the organic layer was washed with water and dried over anhydrous MgSO₄ for 3 h. The solvent was removed by evaporation under reduced pressure. Then the crude product was purified by silica gel column chromatography with dichloromethane/petroleum ether (1:2) as eluent to afford DINDTS as a black solid (59.9 mg, 0.053 mmol, 46.1%, mp 165–166 °C). IR (ν_{max} , cm⁻¹, KBr): 3060 (C-H), 2923 (C-H), 2852 (C-H), 1675 (C=O), 1564, 1459 (C=N, C=C), 1392, 1345, 1149, 1094, 724. ¹H NMR (500 MHz, CDCl₃): δ 7.99–7.94 (m, 4H), 7.90 (s, 2H), 7.80–7.73 (m, 6H), 7.50 (s, 2H), 2.82 (d, *J* = 7.3 Hz, 4H), 1.76 (dd, *J* = 11.7, 5.7 Hz,

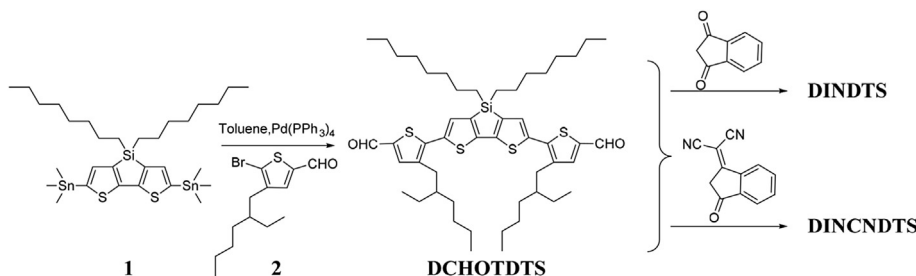
2H), 1.45–1.40 (m, 6H), 1.31 (ddd, *J* = 28.3, 19.4, 10.7 Hz, 34H), 1.02–0.98 (m, 4H), 0.91 (dd, *J* = 13.9, 6.6 Hz, 12H), 0.85 (t, *J* = 6.9 Hz, 6H). ¹³C NMR (126 MHz, CDCl₃) δ 190.47, 189.83, 150.98, 146.44, 146.13, 144.14, 142.04, 140.55, 139.56, 136.93, 135.68, 134.95, 134.74, 134.30, 131.03, 123.61, 122.93, 122.74, 39.64, 33.71, 33.26, 32.57, 31.88, 29.25, 29.15, 28.73, 25.72, 24.15, 23.08, 22.66, 14.16, 14.11, 11.79, 10.68. HRMS (ESI-TOF) *m/z*: calcd for C₆₈H₈₂O₄S₄Si[M]⁺, 1119.4938; found, 1119.4959.

2,2'-((2Z,2'Z)-(((4,4-dioctyl-4H-silolo[3,2-*b*:4,5-*b'*]dithiophene-2,6-diyl)bis(4-(2-ethylhexyl)-thiophene-5,2-diyl))bis(methanlylidene)bis(3-oxo-2,3-dihydro-1*H*-indene-2,1-diylidene))dimalononitrile (DINCNDS): DCHOTDTS (100 mg, 0.116 mmol) and INCN (89.9 mg, 0.464 mmol) was dissolved in a dry CHCl₃ (30 mL) solution under the protection of argon, and then three drops of pyridine was added to the mixture. After stirring and refluxing for 12 h, the mixture was extracted with dichloromethane (50 mL × 2), the organic layer was washed with water and dried over anhydrous MgSO₄ for 3 h. The solvent was removed by evaporation under reduced pressure, the crude product was respectively precipitated from DCM/methanol and DCM/n-hexane to afford DINCNDS as a purple black solid (77.4 mg, 0.064 mmol, 54.9%, mp 216–217 °C). IR (ν_{max} , cm⁻¹, KBr): 3064 (C-H), 2922 (C-H), 2853 (C-H), 2215 (C≡N), 1694 (C=O), 1539, 1425 (C=N, C=C), 1392, 1316, 1135, 1095, 715. ¹H NMR (500 MHz, CDCl₃) δ 8.80 (s, 2H), 8.69 (d, *J* = 6.7 Hz, 2H), 7.93 (d, *J* = 7.2 Hz, 2H), 7.80–7.72 (m, 4H), 7.59 (d, *J* = 16.6 Hz, 4H), 2.82 (d, *J* = 6.9 Hz, 4H), 1.76 (d, *J* = 5.8 Hz, 2H), 1.47–1.25 (m, 38H), 1.04–0.98 (m, 4H), 0.95–0.78 (m, 20H). ¹³C NMR (126 MHz, CDCl₃) δ 8.80, 8.70, 8.69, 7.94, 7.92, 7.79, 7.77, 7.76, 7.74, 7.73, 7.61, 7.58, 2.82, 2.81, 1.77, 1.76, 1.43, 1.42, 1.40, 1.39, 1.37, 1.34, 1.33, 1.31, 1.30, 1.25, 1.03, 1.01, 0.99, 0.93, 0.92, 0.90, 0.89, 0.86, 0.85, 0.83. HRMS (ESI-TOF) *m/z*: calcd for C₇₄H₈₂N₄O₂S₄Si[M]⁺, 1215.5163; found, 1215.5104.

3. Results and discussion

3.1. Synthesis and thermal stability

As shown in Scheme 1, the intermediates of dialdehyde DCHOTDTS was synthesized using Stille coupling, and the target molecules DINDTS and DINCNDS were then prepared by Knoevenagel condensation of DCHOTDTS with end-capped blocks. TGA was used to characterize the thermal stability of these two compounds and the TGA curves were shown in Fig. 2a. As depicted in Fig. 2a, both DINDTS and DINCNDS exhibit good thermal stability with a 5% weight loss (*T_d*) greater than 340 °C under N₂ atmosphere, which is adequate for application in OPVs. DSC analysis (Fig. 2b) shows clear melting points (*T_m*) on the heating process and recrystallization points (*T_{cr}*) on the cooling process, indicating that both DINDTS and DINCNDS possess good crystallization. Larger *T_m* and *T_{cr}* for DINCNDS demonstrate its better crystallization than that of DINDTS.



Scheme 1. Synthetic routes to target molecules.

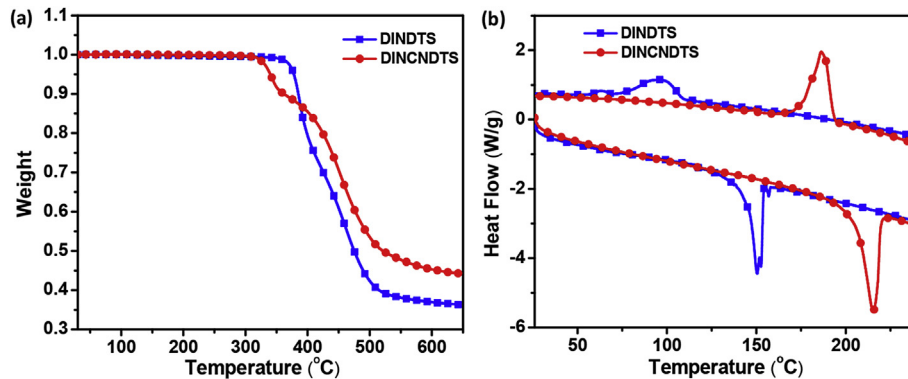


Fig. 2. (a) TGA curves of DINDTS and DINCNCTS; (b) DSC thermograms of DINDTS and DINCNCTS with a heating rate of $10\text{ }^{\circ}\text{C min}^{-1}$ under N_2 . The lower lines and the upper lines are from the heating scans and cooling scans, respectively.

3.2. Optoelectronic and electrochemical properties

The UV-Vis absorption spectra of DINDTS and DINCNCTS in dilute chloroform solution and in solid films are shown in Fig. 3. From Fig. 3a, in chloroform solution, DINDTS shows an absorption peak at 590 nm with a maximum absorption coefficient of $6.49 \times 10^4 \text{ M}^{-1} \text{ cm}^{-1}$, and DINCNCTS presents an absorption peak at 685 nm with a maximum absorption coefficient of $7.68 \times 10^4 \text{ M}^{-1} \text{ cm}^{-1}$. In the solid state, the DINDTS film exhibits an absorption peak at 610 nm, which is red-shifted by 37 nm compared to its solution absorption. DINCNCTS shows a red shift of 67 nm with maximum absorption peak at 722 nm. The red shifts are attributed to intermolecular interaction of these two molecules. Besides, the absorption spectrum of DINCNCTS film presents a shoulder peak at 786 nm, indicative of effective π - π stacking. The optical band gap of DINDTS estimated from the onset of the film absorption spectrum is 1.64 eV, which is larger than that of DINCNCTS (1.39 eV) (Table 1).

The electrochemical properties of DINDTS and DINCNCTS were investigated by CV. The potentials were internally calibrated using the ferrocene/ferrocenium (Fc/Fc^+) of the redox couple (4.8 eV below the vacuum level). Some important data are summarized in Table 1. As shown in Fig. 3c, the HOMO and LUMO energy levels, calculated from the onset oxidation and reduction potential of the redox curves, are -5.01 and -3.40 eV for DINDTS, and -5.08 and -3.62 eV for DINCNCTS, respectively. The electrochemical band gaps of DINDTS and DINCNCTS are estimated to be 1.61 and 1.46 eV, which are consistent with the optical band gaps. These results are also in agreement with the density functional theory

Table 1
Optical and electrochemical data of the compounds.

Compound	$\lambda_{\text{max, sol}}$ (nm)	$\lambda_{\text{max, film}}$ (nm)	λ_{onset} (nm)	$E_g^{\text{opt, film}}$ (eV)	HOMO (eV)	LUMO (eV)	E_g (eV)
DINDTS	590	610	754	1.64	-5.01	-3.40	1.61
DINCNCTS	685	722	894	1.39	-5.08	-3.62	1.46

(DFT) calculation results using the B3LYP/6-31G(d) model (Fig. S1). These results show that these two molecules possess slightly lower HOMO energy levels compared to the reported DTS based small molecules, which is associated with the shorter π -bridges [10]. For OSCs, the open-circuit voltage (V_{oc}) is closely related to the difference between the HOMO energy level of donor material and the LUMO energy level of acceptor materials [28]. Thus, higher V_{oc} would be expected for OSCs. Besides, from Table 1, we can see that the smaller band gap for DINCNCTS mainly resulted from its lower LUMO energy level, which is due to the stronger electron-withdrawing ability of the terminal acceptor INCN.

3.3. Photovoltaic performance

BHJ organic solar cells were fabricated using DINDTS and DINCNCTS as the electron donors with a standard device structure of ITO/PEDOT:PSS/donor:PC₇₁BM/ETL-1/Al and tested under AM 1.5G illumination at an intensity of 100 mW cm^{-2} . ETL-1 is an efficient methanol-soluble fullerene-based electron-extraction-layer material [29], and its structure is shown as Fig. S2. The characteristic current density vs voltage (J - V) curves are presented in

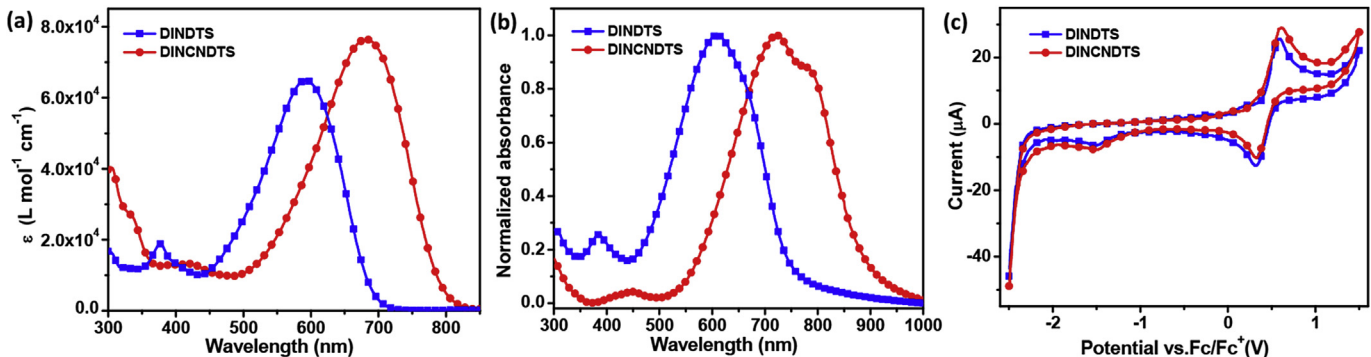


Fig. 3. (a) Absorption spectra of DINDTS and DINCNCTS in chloroform solution; (b) Normalized absorption spectra of DINDTS and DINCNCTS films; (c) Cyclic voltammograms of DINDTS and DINCNCTS in THF solutions of $0.1 \text{ mol L}^{-1} \text{ Bu}_4\text{NPF}_6$ with a scan rate of 100 mV s^{-1} .

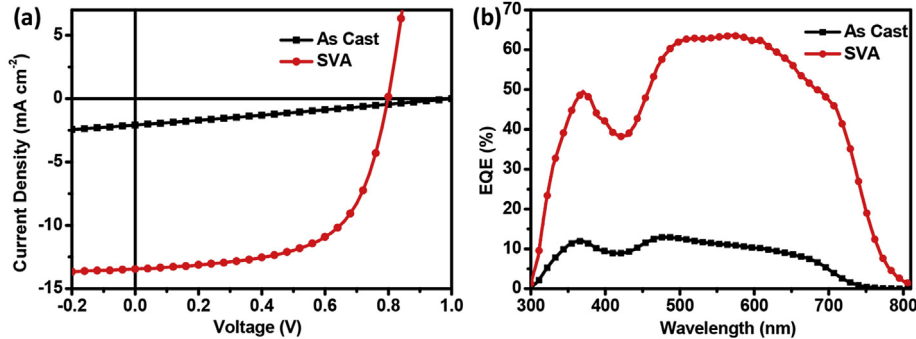


Fig. 4. (a) Typical *J-V* curves of DINDTS based devices as-cast or with SVA treatment. (b) The EQE curves of DINDTS based devices as-cast or with SVA treatment.

Table 2

The photovoltaic parameters of DINDTS and DINCNNTS based devices with or without SVA treatment.

Compound	Treatment	V _{oc} (V)	J _{sc} (mA cm ⁻²)	FF (%)	PCE (%)
DINDTS	None	1.005	2.27	26.2	0.60
	SVA	0.799	13.50	61.2	6.60
DINCNNTS	None	0.857	1.82	37.3	0.58
	SVA	0.824	1.69	36.3	0.51

Fig. 4a and the photovoltaic parameters are summarized in Table 2. Without any post-treatment, the DINDTS:PC₇₁BM devices gave a high V_{oc} of 1.005 V, a J_{sc} of 2.27 mA cm⁻², an FF of 26.2% and a PCE of 0.60%. The high V_{oc} results from its lower HOMO. After SVA treatment with chloroform as the solvent, the PCE of the DINDTS based device was sharply enhanced to 6.60%, with an improved J_{sc} of 13.50 mA cm⁻² and FF of 61.2%, which is closely associated with the better developed morphology as discussed below. In comparison, the as-cast DINCNNTS:PC₇₁BM based devices exhibited a poor PCE of 0.58% with a low J_{sc} of 1.82 mA cm⁻². However, from Table 2, it can be seen that SVA treatment didn't work for it. For its relatively low LUMO energy levels, DINCNNTS has also been used as electron

acceptors with some excellent polymer donors for organic solar cells; nevertheless, the photovoltaic performances are still poor (Table S1).

The external quantum efficiency (EQE) curves of the DINDTS based devices are shown in Fig. 4b. As shown in Fig. 4b, without post-treatment, the devices exhibited relatively low EQE with maximum value below 15%. After SVA treatment, uniform increases in the spectral response across the wavelength range of 300–800 nm are clearly observed. The calculated J_{sc} obtained by integration of the EQE curves are 2.16 and 12.94 mA cm⁻² for the as-cast and the optimized devices, respectively, which are within 5% mismatch compared with the values got from the J-V curves.

3.4. Film morphology and hole mobility

To understand the effect of SVA treatment on the device performance, atomic force microscopy (AFM) and transmission electron microscopy (TEM) were used to characterize the morphologies of the active layers. From Fig. 5a and b, the surface root-mean-square (RMS) roughness are 1.60 and 1.30 nm for the as-cast and SVA-treated DINDTS:PC₇₁BM blend films, respectively. For the as-

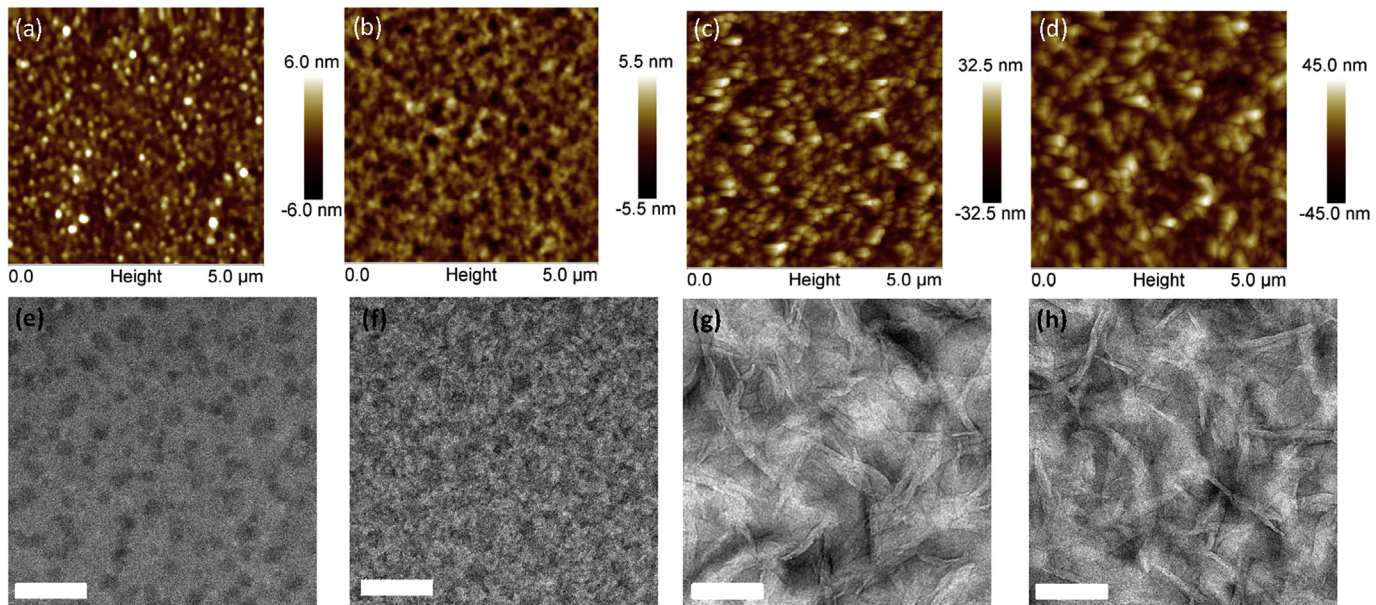


Fig. 5. Tapping-mode AFM height images of DINDTS:PC₇₁BM blend films (a) as cast and (b) with SVA treatment; AFM images of DINCNNTS:PC₇₁BM blend films (c) as cast and (d) with SVA treatment. TEM images of DINDTS:PC₇₁BM blend films (e) as cast and (f) with SVA treatment; TEM images of DINCNNTS:PC₇₁BM blend films (g) as cast and (h) with SVA treatment. (Scale bar is 200 nm).

cast film, there are many large aggregates with size over 50 nm, which are detrimental for exciton diffusion and dissociation and thus lead to poor J_{sc} . The discontinuous phase aggregation could cause severe bimolecular recombination, which leads to low FF. After SVA treatment, good interpenetrating network of donor/acceptor in the blend film was developed, which could be helpful for exciton dissociation and charge transport, and therefore J_{sc} and FF were greatly improved. For TEM images, the dark regions could be assigned to PCBM domains because of its relatively high electron scattering density, and the light regions are referred to the donor domains [30]. As depicted in Fig. 5e and f, after SVA treatment, large aggregates disappeared and a bi-continuous interpenetrating network could be observed. All of these are beneficial for getting larger J_{sc} and FF, and thus higher PCE. However, from the AFM images of DINCNDTS:PC₇₁BM active layers as shown in Fig. 5c and d, the RMS roughness for the as-cast and SVA-treated films are 8.03 and 11.20 nm, respectively, which are not smooth and suggest that SVA treatment didn't make much different. Similarly, large aggregates could be observed in the TEM images, which may be due to its high crystallinity, and these gave rise to low exciton dissociation and charge collection efficiency, therefore small J_{sc} and FF. The low J_{sc} may also be partly due to the small LUMO energy level offset between DINCNDTS and PC₇₁BM, which could not provide sufficient driving force to separate excitons. This is also demonstrated by its lower photoluminescence quenching efficiency of 27.8% (Fig. S3).

The hole mobility is also an important parameter for photovoltaic performance. Therefore, the hole mobility for DINDTS in the hole only devices with a device structure of ITO/PEDOT:PSS/DINDTS:PC₇₁BM/Au by using the space charge limited current (SCLC) method were measured. The J - V characteristics of the hole-only DINDTS based devices with or without SVA treatment in the dark are shown in Fig. S4. Hole mobility for the as-cast device is $4.48 \times 10^{-5} \text{ cm}^2 \text{ V}^{-1} \text{ s}^{-1}$. After SVA treatment, the hole mobility was improved to be $1.31 \times 10^{-3} \text{ cm}^2 \text{ V}^{-1} \text{ s}^{-1}$, which contributed to its improved FF.

4. Conclusion

In conclusion, two small molecules based on DTS unit were designed and synthesized for solution processed organic solar cells. DINCNDTS exhibited broad absorption extending to over 900 nm. However, the relatively poor morphology of DINCNDTS:PC₇₁BM blend film leads to smaller J_{sc} and FF, and thus poor PCE. DINDTS with a terminal group possessing relatively weak electron withdrawing ability gave good performance. The optimized DINDTS based devices exhibited a PCE of 6.60%, which is due to the better developed interpenetrating network after SVA treatment. These results suggest that the end-capped blocks have a great impact on the band gap and fine-tuned morphology, together with the photovoltaic performance.

Acknowledgements

The authors gratefully acknowledge financial support from the Startup Research Fund of Hangzhou Normal University (No. PD02003003002003), National Natural Science Foundation of China (NSFC) (Nos. 21274034, 21074028 and 21574034), and the Natural Science Foundation of Zhejiang Province (ZJNSF) (No. LY16B040006).

The authors declare no conflict of interest.

Appendix A. Supplementary data

Supplementary data related to this article can be found at <http://dx.doi.org/10.1016/j.dyepig.2017.07.059>.

References

- [1] Service RF. Outlook brightens for plastic solar cells. *Science* 2011;332(6027):293.
- [2] Deng D, Zhang Y, Zhang J, Wang Z, Zhu L, Fang J, et al. Fluorination-enabled optimal morphology leads to over 11% efficiency for inverted small-molecule organic solar cells. *Nat Commun* 2016;7:13740.
- [3] Kan B, Li M, Zhang Q, Liu F, Wan X, Wang Y, et al. A series of simple oligomer-like small molecules based on oligothiophenes for solution-processed solar cells with high efficiency. *J Am Chem Soc* 2015;137(11):3886–93.
- [4] Gao K, Miao J, Xiao L, Deng W, Kan Y, Liang T, et al. Multi-length-scale morphologies driven by mixed additives in porphyrin-based organic photovoltaics. *Adv Mater* 2016;28:4727–33.
- [5] Xu S, Zhou Z, Fan H, Ren L, Liu F, Zhu X, et al. An electron-rich 2-alkylthieno[3,4-B]thiophene building block with excellent electronic and morphological tunability for high-performance small-molecule solar cells. *J Mater Chem A* 2016;4(44):17354–62.
- [6] Wang J-L, Liu K-K, Yan J, Wu Z, Liu F, Xiao F, et al. Series of multifluorine substituted oligomers for organic solar cells with efficiency over 9% and fill factor of 0.77 by combination thermal and solvent vapor annealing. *J Am Chem Soc* 2016;138(24):7687–97.
- [7] Zhao J, Li Y, Yang G, Jiang K, Lin H, Ade H, et al. Efficient organic solar cells processed from hydrocarbon solvents. *Nat Energy* 2016;1:15027.
- [8] He Z, Xiao B, Liu F, Wu H, Yang Y, Xiao S, et al. Single-junction polymer solar cells with high efficiency and photovoltage. *Nat Photonics* 2015;9(3):174–9.
- [9] Zuo L, Chang C-Y, Chueh C-C, Zhang S, Li H, Jen AKY, et al. Design of a versatile interconnecting layer for highly efficient series-connected polymer tandem solar cells. *Energy Environ Sci* 2015;8(6):1712–8.
- [10] Chen W, Zhang Q. Recent progress in non-fullerene small molecule acceptors in organic solar cells (OSCs). *Dyes Pigments* 2015;122:231–7.
- [11] Wang C, Okabe T, Long G, Kuzuhara D, Zhao Y, Aratani N, et al. A novel d-π-a small molecule with N-Heteroacene as acceptor moiety for photovoltaic application. *J Mater Chem C* 2015;3:4698–705.
- [12] Chen W, Salim T, Fan H, James L, Lam Y-M, Zhang Q, et al. Quinoxaline-functionalized C₆₀ derivatives as electron acceptors in organic solar cells. *J Mater Chem C* 2017;5:1275–302.
- [13] Chen W, Yang X, Long G, Wan X, Chen Y, Zhang Q, et al. A perylene diimide (PDI)-Based small molecule with tetrahedral configuration as a non-fullerene acceptor for organic solar cells. *RSC Adv* 2014;4:25291–301.
- [14] Collins SD, Ran NA, Heiber MC, Nguyen T-Q. Small is powerful: recent progress in solution-processed small molecule solar cells. *Adv Energy Mater* 2017. <http://dx.doi.org/10.1002/aenm.201602242>.
- [15] Wang Z, Xu X, Li Z, Feng K, Li K, Li Y, et al. High efficiently halogen-free solvent processed small-molecule organic solar cells enabled by material design and device engineering. *Energy Environ Sci* 2017. <http://dx.doi.org/10.1039/c7ee00805h>.
- [16] Cui C, Guo X, Min J, Guo B, Cheng X, Zhang M, et al. High-performance organic solar cells based on a small molecule with alkylthio-thienyl-conjugated side chains without extra treatments. *Adv Mater* 2015;27(45):7469–75.
- [17] Coughlin JE, Henson ZB, Welch GC, Bazan GC. Design and synthesis of molecular donors for solution-processed high-efficiency organic solar cells. *Acc Chem Res* 2014;47(1):257–70.
- [18] Li W, Deng W, Wu K, Xie G, Yang C, Wu H, et al. The end-capped group effect on dithienosilole trimer based small molecules for efficient organic photovoltaics. *J Mater Chem C* 2016;4(10):1972–8.
- [19] Ni W, Li M, Liu F, Wan X, Feng H, Kan B, et al. Dithienosilole-based small-molecule organic solar cells with an efficiency over 8%: investigation of the relationship between the molecular structure and photovoltaic performance. *Chem Mater* 2015;27(17):6077–84.
- [20] Liu C, Wang K, Gong X, Heeger AJ. Low bandgap semiconducting polymers for polymeric photovoltaics. *Chem Soc Rev* 2015;45(17):4825.
- [21] Lu LY, Zheng TY, Wu QH, Schneider AM, Zhao DL, Yu LP. Recent advances in bulk heterojunction polymer solar cells. *Chem Rev* 2015;115(23):12666–731.
- [22] Huang Y, Kramer EJ, Heeger AJ, Bazan GC. Bulk heterojunction solar cells: morphology and performance relationships. *Chem Rev* 2014;114(14):7006–43.
- [23] Li M, Liu F, Wan X, Ni W, Kan B, Feng H, et al. Subtle balance between length scale of phase separation and domain purification in small-molecule bulk-heterojunction blends under solvent vapor treatment. *Adv Mater* 2015;27(40):6296–302.
- [24] Wessendorf CD, Schulz GL, Mishra A, Kar P, Ata I, Weideler M, et al. Efficiency improvement of solution-processed dithienopyrrole-based a-d-a oligothiophene bulk-heterojunction solar cells by solvent vapor annealing. *Adv Energy Mater* 2014;4(14):1400266.
- [25] Liao HC, Tsao CS, Huang YC, Jao MH, Tien KY, Chuang CM, et al. Insights into

- solvent vapor annealing on the performance of bulk heterojunction solar cells by a quantitative nanomorphology study. *RSC Adv* 2014;4(12):6246–53.
- [26] Chen H, Hsiao Y-C, Hu B, Dadmun M. Control of morphology and function of low band gap polymer-bis-fullerene mixed heterojunctions in organic photovoltaics with selective solvent vapor annealing. *J Mater Chem A* 2014;2(25): 9883–90.
- [27] Min J, Jiao X, Ata I, Osvet A, Ameri T, Bäuerle P, et al. Time-dependent morphology evolution of solution-processed small molecule solar cells during solvent vapor annealing. *Adv Energy Mater* 2016;6(10):1502579.
- [28] Scharber MC, Mühlbacher D, Koppe M, Denk P, Waldauf C, Heeger AJ, et al. Design rules for donors in bulk-heterojunction solar cells-towards 10% energy-conversion efficiency. *Adv Mater* 2006;18(6):789–94.
- [29] Li CZ, Chueh CC, Yip HL, O'malley KM, Chen WC, Jen AKY. Effective interfacial layer to enhance efficiency of polymer solar cells via solution-processed fullerene-surfactants. *J Mater Chem* 2012;22(17):8574–8.
- [30] Yang X, Loos J, Veenstra SC, Verhees WJH, Wienk MM, Kroon JM, et al. Nanoscale morphology of high-performance polymer solar cells. *Nano Lett* 2005;5(4):579–83.